$FeMn_3Ge_2Sn_7O_{16}$: a Perfectly Isotropic 2-D Kagomé Lattice that Breaks Magnetic Symmetry with Partial Spin Order

Morgan C. Allison,[a,b] Sabine Wurmehl,[b] Bernd Büchner,[b] Joseph L. Vella,[c] Tilo Söhnel,[c] Sascha A. Bräuninger,[d] Hans-Henning Klauss,[d] Maxim Avdeev,[a,e] Frederick P. Marlton,[a] Siegbert Schmid,[a] and Chris D. Ling*[a]

[a] School of Chemistry, The University of Sydney, Sydney 2006, Australia

[b] Institute for Solid State Research, Leibniz IFW Dresden, Helmholtzstr. 20, 01069 Dresden, Germany

[c] School of Chemical Sciences, University of Auckland, Auckland 1142, New Zealand

[d] Institute of Solid State and Materials Physics, University of Dresden, 01069 Dresden, Germany

[e] Australian Centre for Neutron Scattering, ANSTO, Menai 2234, Australia

ABSTRACT: $FeMn_3Ge_2Sn_7O_{16}$ is a fully ordered stoichiometric phase containing an undistorted hexagonal kagomé lattice of Mn^{2+} cations. It represents not only an important expansion of the chemistry of the complex composite $FeFe_3Si_2Sn_7O_{16}$ structure type, by replacing silicon with germanium, but also an improvement on the perfection of the kagomé lattice by replacing anisotropic high-spin Fe^{2+} (d^6, L = 2) with isotropic high-spin Mn^{2+} (d^5, L = 0), controlled by the size-matched replacement of SiO_4^{4-} with GeO_4^{4-} bridging units. This anisotropy was suspected of playing a role in the unique 'striped' magnetic structure of $FeFe_3Si_2Sn_7O_{16}$ at low temperatures, which breaks hexagonal symmetry and leaves one-third of the magnetic moments geometrically frustrated and fluctuating down to at least 0.1 K. We observe the same striped magnetic structure in $FeMn_3Ge_2Sn_7O_{16}$, ruling out single-ion anisotropy as the driving force and deepening the intrigue around the apparent 'partial spin-liquid' nature of these compounds.

Introduction

A core goal of solid-state chemistry is the rational design of new compounds with specific arrangements and choice of elements, which are expected to give rise to desired physical properties. Those properties may be of technological or fundamental interest. Into the latter category fall low-dimensional and geometrically frustrated magnetic (GFM) materials, where magnetic atoms or ions are strongly exchange-coupled but their topology and/or symmetry of interactions suppress conventional long-range order, so that exotic ground states such as quantum spin-liquids (QSLs)[1, 2] can emerge.

The archetypal low-dimensional GFM topologies are the simple triangular lattice[3, 4] and the expanded triangular kagomé lattice.[5-7] Antiferromagnetic (AFM) exchange interactions among Ising (colinear) unpaired spins on these lattices cannot be satisfied for all nearest neighbours simultaneously. A conventional unique long-range ordered ground state is therefore replaced by a macroscopic number of degenerate ground states, which will either freeze into a spin-ice or continue to fluctuate as a QSL (see reviews in [8-10]). In practice, QSLs are elusive because most real compounds with these lattice topologies do not maintain perfectly hexagonal (trigonal) symmetry at low temperatures, breaking the degeneracy and permitting long-range order; and/or the unpaired spins become non-colinear, in which case long-range order is possible (e.g., the $q = 0$ and $\sqrt{3}\times\sqrt{3}$ states on the kagomé lattice[11]).

$Fe_4Si_2Sn_7O_{16}$ is a striking exception.[12] Its structure (Figure 1a) contains an ionic-type layer of edge-sharing FeO_6 and $Sn^{4+}O_6$ octahedra, forming a kagomé lattice of magnetic Fe^{2+} cations (high-spin [HS] d^6, $S = 2$) with perfect trigonal symmetry. The kagomé layers alternate with layers of intermetallic character based on $FeSn^{2+}{}_6$ octahedra, which we shall refer to as the stannide layer, and which is non-magnetic because the Fe^{2+} is in the low-spin (LS) state, experimentally confirmed by Mössbauer spectroscopy.[13, 14] These layers are bridged/separated by SiO_4 tetrahedra. The formula can be written as $FeFe_3Si_2Sn_7O_{16}$ to differentiate the one LS-Fe^{2+} per formula unit in the stannide layer from the three HS-Fe^{2+} per formula unit in the kagomé oxide layer.

Below the ordering temperature $T_N = 3.5$ K, the spins on 2/3 of the Fe^{2+} sites in the kagomé oxide layers order antiferromagnetically, while the other 1/3 remain disordered and fluctuating down to at least 0.1 K.[13, 14] The origin of this unique "striped" state is unclear. The fact that it breaks trigonal symmetry, which the well-known $q = 0$ and $\sqrt{3}\times\sqrt{3}$ states do not, raises the possibility that the magnetic anisotropy of L = 2 HS-Fe^{2+} ($t_{2g}^4e_g^2$) plays a role. The obvious way to test this hypothesis is to remove an electron by replacing HS-Fe^{2+} in the kagomé lattice with L = 0 HS-Mn^{2+} ($t_{2g}^3e_g^2$), while retaining non-magnetic LS-Fe^{2+} in the stannide layer. However, attempts to synthesise $FeMn_3Si_2Sn_7O_{16}$ were only partially successful, the maximum achievable Mn content being $Fe(Fe_{0.45}Mn_{2.55})Si_2Sn_7O_{16}$.[15] Samples of this composition had the same striped magnetic ground state below a slightly reduced $T_N = 2.5$ K; however, the continued presence of some HS-Fe^{2+} in the kagomé lattice did not rule out the possibility that the HS-Fe^{2+} magnetic anisotropy is the key driver for that state.

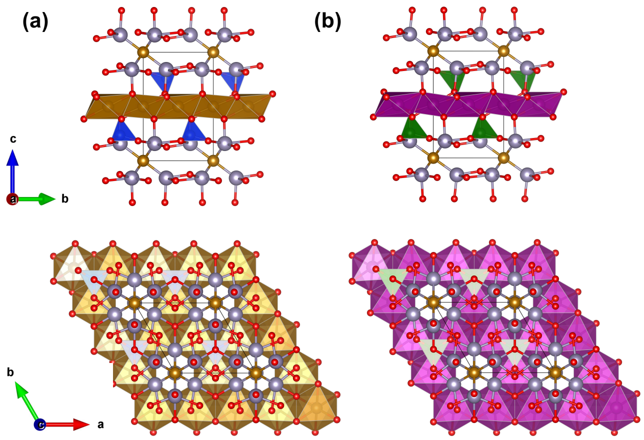

Figure 1. Structures of (a) $FeFe_3Si_2Sn_7O_{16}$ [12] and (b) $FeMn_3Ge_2Sn_7O_{16}$ [this work], Rietveld-refined against neutron powder diffraction data. The space group in both cases is trigonal *P*-3*m*1 (#164). Fe atoms and FeO_6 (MnO_6) octahedra are gold (purple), Sn atoms are grey, SiO_4 (GeO_4) tetrahedra are blue (green), and O atoms are red.

From a crystal-chemical perspective, the limitation on Mn content is most likely a question of size-matching between the kagomé layer and its facing layers, which consist of SiO_4 tetrahedra and $FeSn_6$ octahedra. In an octahedral crystal field, the effective ionic radius (IR) of HS-Mn^{2+} is 0.83 Å, vs. 0.78 Å for HS-Fe^{2+}.[16] Because the facing/bridging layers have relatively strict bond-length requirements (especially the largely covalent SiO_4 tetrahedra), the kagomé layer can only expand along the *c* axis as Mn is substituted for Fe, while the *a*-*b* plane remains fixed. This distorts the MnO_6 octahedra, and the tolerance for that distortion falls slightly short of complete substitution.

To achieve complete HS-Mn^{2+} substitution into the kagomé layer, we therefore need to expand the facing layers in the *a*-*b* plane. Noting that tin is present as both Sn^{2+} and Sn^{4+}, and this behaviour is clearly central to its chemical stability, our approach was to co-substitute Ge^{4+} (tetrahedral IR = 0.39 Å) for Si^{4+} (0.26 Å).[16]

Experimental

Samples were prepared by a solid-state ceramic oxide sintering method. Stoichiometric amounts of high purity (≥99.9%) Fe_2O_3, MnO, GeO_2 oxides and Sn metal powder were ground together using an agate mortar and pestle before loading into an alumina crucible with a small amount of Sn metal as an oxygen buffer, then sealing the crucible inside a quartz tube in air. The quartz tube was then heated to 1023 K for 72 hours, before quenching in water to room temperature.

X-ray powder diffraction (XRPD) patterns were collected using non-monochromatic Cu K_α radiation on a Panalytical MPD X-ray powder diffractometer over the range 5 to 90° 2θ with a step size of 0.01315° 2θ. The structural models were refined against these data using the Rietveld method as implemented in Topas[17] (in combination with ISODISTORT[18] for the magnetic structures). Neutron powder diffraction (NPD) data were collected using the Echidna[19] diffractometer at the Australian Centre for Neutron Scattering, Lucas Heights, Australia. NPD data were collected from a ~5 g sample placed in a 6 mm diameter vanadium can. Room-temperature NPD data were collected using $\lambda = 1.6215$ Å neutrons to maximize high-Q coverage for refinement of structural details. Low-temperature and in-field (up to 10 T) NPD data were collected using $\lambda = 2.4395$ Å neutrons to maximise resolution of magnetic Bragg peaks at low Q, in a cryomagnet with a ^{3}He-dilution insert to reach the lowest possible temperatures.

Zero field-cooled (ZFC) and field-cooled (FC) temperature-dependent DC magnetic susceptibility measurements were carried out in Quantum Design Physical Properties Measurement System (PPMS) using the vibrating sample magnetometer (VSM) attachment, in a 0.1 T applied field, between room temperature and 2 K. Field-dependent magnetization was measured at 1.9 and 10.0 K using the same instrument configuration over a field range ±8 T.

^{57}Fe-Mössbauer measurements were carried out in a Cryo Vac helium flow cryostat with 6 L helium volume protected by a nitrogen heat shield. For the room-temperature measurement, all pumps were deactivated to avoid broadening by vibrations. We used commercial NIM rack devices. The drive was a Mössbauer WissEL drive unit MR-360 biased by a DFG-500 frequency generator in sinusoidal mode. Data were recorded with a CMTE multichannel data processor MCD 301/8K and a WissEL single channel analyzer Timing SCA to select the energy window. The detector was a proportional counter tube and the source a Rh/Co source with an initial activity of 1.4 GB. The sample was a powder and prepared with a sample thickness of 0.57 g cm^{-2} parallel to the beam. Data were analyzed with the software package Moessfit.[20]

Results and Discussion

Samples of stoichiometry $FeFe_3Ge_2Sn_7O_{16}$, $FeMn_3Ge_2Sn_7O_{16}$, and $MnMn_3Ge_2Sn_7O_{16}$, were initially heated in sealed quartz ampoules at 1173 K as for the silicate analogues,[15] but the higher vapour pressure of Ge vs. Si [21] led to significant Ge loss to the gas phase. This problem was resolved when the synthesis temperature was reduced to 1023 K. XRPD patterns of the $FeMn_3Ge_2Sn_7O_{16}$ sample showed the desired trigonal phase as the main product, accompanied by an SnO_2 impurity due to the Sn excess required for synthesis. The SnO_2 can be removed by successive washing with 50% diluted fuming HCl; however, given that it is non-magnetic with a small unit cell, and therefore easily accounted for in all our other experimental methods, we chose not to risk degrading the sample quality of the target phase by subjecting it to this aggressive treatment. There was no sign of the desired trigonal phase in the $FeFe_3Ge_2Sn_7O_{16}$ and $MnMn_3Ge_2Sn_7O_{16}$ samples.

The structure of $FeMn_3Ge_2Sn_7O_{16}$ was initially Rietveld-refined against XRPD data starting from the published model of $FeFe_3Si_2Sn_7O_{16}$, with all Si replaced by Ge and all the Fe in the kagomé oxide layer replaced by Mn. Instrumental and unit cell parameters, the fraction of SnO_2 impurity, atomic coordinates and atomic displacement parameters (ADPs) could be reliably refined, while the occupancy of the transition metal sites was fixed at the expected nominal composition due to the insensitivity of X-rays to the difference between Fe and Mn. The final Rietveld-refinement was therefore carried out against room-temperature 1.6215 Å NPD data, to take advantage of the very different coherent neutron scattering lengths of Fe and Mn (9.45 and –3.73 fm, respectively). Site occupancies in the kagomé oxide layer refined to 100% Mn, and in the stannide layer to 100% Fe, within error (2%), and were subsequently fixed at these values – i.e., the stoichiometry was confirmed as $FeMn_3Ge_2Sn_7O_{16}$. Refinement against NPD data also yielded more reliable fractional coordinates and atomic displacement parameters (ADPs) for the relatively light oxygen atoms, compared to XRPD data. The final Rietveld fit is shown in Figure 2. Details of the refined structure have been deposited as a Crystallographic Information File (CIF) (CCDC Deposition Number 2078879).

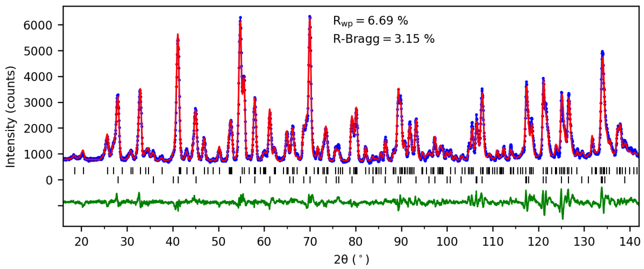

Figure 2. Rietveld fit to room-temperature 1.6215 Å NPD data for $FeMn_3Ge_2Sn_7O_{16}$. The lower reflection markers refer to the SnO_2 impurity.

Further evidence that all the Fe in $FeMn_3Ge_2Sn_7O_{16}$ is located exclusively in the stannide layer comes from ^{57}Fe-Mössbauer spectroscopy. Figure 3 shows a room-temperature Mössbauer spectrum and the corresponding fit, which exhibits a single absorption line. Compared to previously published results for $Fe_4Si_2Sn_7O_{16}$,[12, 13] the background scattering is high due to the low Fe content and the high absorption coefficients of Mn (53 cm² g^{-1}) and Ge (102 cm² g^{-1}) with respect to the 14.4 keV transition.[22] The isomer shift δ = 0.35(1) mm s^{-1} relative to α-Fe value is within error bars identical to the LS-Fe^{2+} $S = 0$ site observed in the stannide layer in $Fe_4Si_2Sn_7O_{16}$[13]. The HWHM linewidth is 0.165(10) mm s^{-1}. In $Fe_4Si_2Sn_7O_{16}$ the Fe^{2+} $S = 0$ site exhibits a quadrupole splitting of Δ = 0.48 mm s^{-1}, in $FeMn_3Ge_2Sn_7O_{16}$ Δ is one order of magnitude smaller and consistent with zero indicating a higher symmetry Fe^{2+} environment in the stannide layer. (Note that while the Fe and Mn compounds are isostructural, the *P*-3*m*1 space group does not constrain the $FeSn_6$ octahedra to be perfectly regular: Fe–Sn bond lengths are identical, but Sn–Fe–Sn bond angles are split into two sets at 92.4° and 87.6° for $Fe_4Si_2Sn_7O_{16}$, vs. a much more symmetric 90.8° and 89.2° for $FeMn_3Ge_2Sn_7O_{16}$).

The Rietveld-refined structure of $FeMn_3Ge_2Sn_7O_{16}$ is compared to that of $FeFe_3Si_2Sn_7O_{16}$ in Figure 1. They are entirely isostructural. The unit cell parameters are compared to those of $FeFe_3Si_2Sn_7O_{16}$ and partially Mn-doped silicates [15] in Table 1. The observed changes are perfectly consistent with the crystal-chemical conception of our work. Substituting Ge^{4+} (tetrahedral IR = 0.39 Å) for Si^{4+} (0.26 Å) allows the lattice to expand 1.9% in $a = b$ but only 0.1% in c, allowing HS-Mn^{2+} (octahedral IR = 0.83 Å) to fully substitute for HS-Fe^{2+} (0.78 Å) in the kagomé oxide layer. This contrasts with previous attempts to directly substitute Mn for Fe in $FeFe_3Si_2Sn_7O_{16}$, where the *a*-*b* plane was relatively constrained, and full substitution could not be achieved.[15] The fact that we could not synthesise $FeFe_3Ge_2Sn_7O_{16}$ in this work is further consistent with this logic, applied in reverse: the expanded GeO_4 layer is incompatible with an Fe^{2+} kagomé layer. The fact that we could also not synthesize $MnMn_3Ge_2Sn_7O_{16}$ may be due to LS-Fe^{2+} ($t_{2g}^6e_g^0$) being particularly stable in the intermediate layer site, surrounded by Sn^{2+} cations.

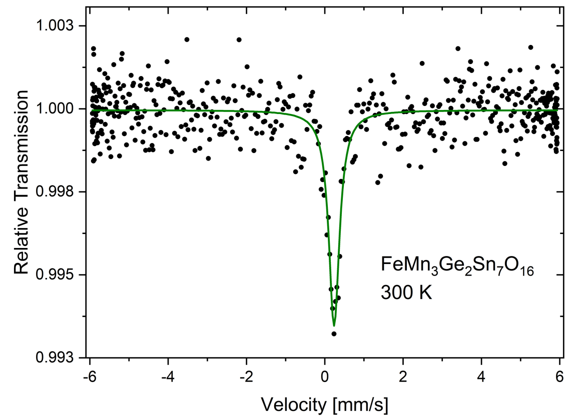

Figure 3. ^{57}Fe-Mössbauer measurement at room temperature of $FeMn_3Ge_2Sn_7O_{16}$ measured for eight days (data points are black) and the fit of the static powder Hamiltonian (green line).

Table 1. Unit cell parameters and compositions of trigonal *P*-3*m*1 (#164) Fe*B*$_3$Si$_2$Sn$_7$O$_{16}$ [15] and FeMn$_3$Ge$_2$Sn$_7$O$_{16}$.

Composition	a (Å)	c (Å)	V (Å^3)
$FeFe_3Si_2Sn_7O_{16}$	6.826027(13)	9.14195(3)	368.8973(15)
$Fe(Fe_{2.19}Mn_{0.81})Si_2Sn_7O_{16}$	6.841036(8)	9.147802(17)	370.7585(9)
$Fe(Fe_{1.40}Mn_{1.60})Si_2Sn_7O_{16}$	6.853938(7)	9.155267(16)	372.4619(9)
$Fe(Fe_{0.45}Mn_{2.55})Si_2Sn_7O_{16}$	6.867000(10)	9.16467(2)	374.2669(11)
$FeMn_3Ge_2Sn_7O_{16}$	6.95539(16)	9.1555(5)	383.58(3)

Temperature-dependent DC magnetic susceptibility data curves for $FeMn_3Ge_2Sn_7O_{16}$ are shown in Figure 4. A clear downturn on cooling through T_N = 2.2 K in the zero field-cooled (ZFC) curve, measured on warming (slightly delayed to 2.1 K in the field-cooled (FC) curve, measured on cooling) suggests a long-range-ordered AFM transition, similar to T_N = 3.5 K in $FeFe_3Si_2Sn_7O_{16}$.[13] No significant ZFC-FC divergence is seen, nor any significant opening in the field-dependent magnetisation curves at 1.9 K or 10.0 K (Figure 5), further reminiscent of $FeFe_3Si_2Sn_7O_{16}$. However, a change in behaviour at ~2 T in the 1.9 K data suggests some change in the magnetic structure at higher fields. A standard analytical diamagnetic correction was applied [23] (-1.019×10^{-4} emu mol^{-1}) and the data were well-fitted by the Curie-Weiss law between 300 and 15 K. The parameters extracted from the fit to FC data are shown in Table 2, compared to those of $FeFe_3Si_2Sn_7O_{16}$ and $Fe(Fe_{0.45}Mn_{2.55})Si_2Sn_7O_{16}$. The effective moment μ_{eff} = 6.11 μ_B/Mn is slightly larger than the spin-only moment of 5.92 μ_B/Mn. The discrepancy is within the range typically observed experimentally for octahedral HS-Mn^{2+} compounds; however, we note that a possible source of systematic error is our correction for the mass fraction of non-magnetic SnO_2 impurity, which was determined by Rietveld refinement against NPD data and may be affected by correlations with other refined variables including ADPs and absorption. The magnetic frustration index $f = |\theta/T_N| = 6.0$ for $FeMn_3Ge_2Sn_7O_{16}$, which is significantly higher than $f = 3.6$ for $FeFe_3Si_2Sn_7O_{16}$[13] but still relatively modest.

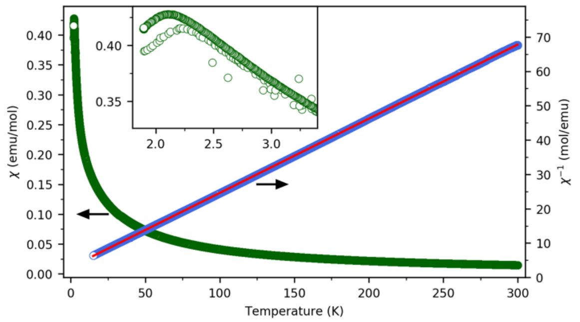

Figure 4. Temperature-dependent DC magnetic susceptibility for $FeMn_3Ge_2Sn_7O_{16}$ in zero field-cooled (ZFC, open circles) and field-cooled (FC, closed circles) modes, taken in an applied field of 0.1 T (green). The right-hand axis shows inverse FC susceptibility (blue) fit to the Curie-Weiss law (magenta) over 300-15 K.

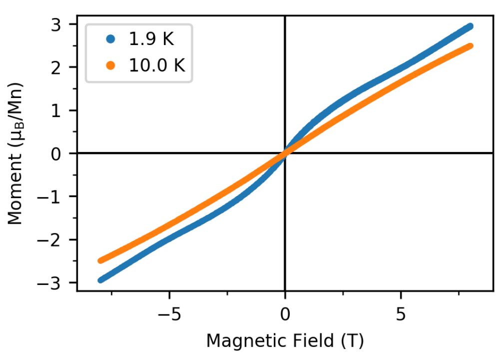

Figure 5. Field-dependent magnetisation of $FeMn_3Ge_2Sn_7O_{16}$ at 1.9 K (blue) and 10 K (orange).

Figure 6 shows low-temperature NPD data at 5 K, 1.6 K, and 0.1 K, focusing on the low-angle region where magnetic scattering is strongest. The broad features (particularly marked at ~35 °2θ) are background from the ^{3}He-dilution insert. Magnetic Bragg peaks below $T_N = 2.2$ K are strongly reminiscent of those seen in $FeFe_3Si_2Sn_7O_{16}$,[13] and indeed are indexed by the same propagation vector $q = (0,½,½)$, with very similar relative intensities. The 1.6 K and 0.1 K data were therefore used to Rietveld-refine the magnetic structure of $FeMn_3Ge_2Sn_7O_{16}$ starting from that of $FeFe_3Si_2Sn_7O_{16}$, in the Shubnikov magnetic space group (Opechowski-Guccione setting) $C2_c2/m$, No. 12.6.71.

Table 2. Magnetic properties of selected Fe*B*$_3$Si$_2$Sn$_7$O$_{16}$-type phases, from Curie-Weiss fits to field-cooled temperature-dependent DC magnetic susceptibility data.

Composition	T_N (K)	θ (K)	μ_{eff} (μ_B/B)	μ_{so} (μ_B/B)
$FeFe_3Si_2Sn_7O_{16}$	3.5	-12.7	5.45	4.90
$Fe(Fe_{0.45}Mn_{2.55})Si_2Sn_7O_{16}$	2.5	-14.5	6.04	5.76
$FeMn_3Ge_2Sn_7O_{16}$	2.2	-13.2	6.11	5.92

Figure 7a shows the final combined nuclear and magnetic fit at 0.1 K, with an ordered moment in the *x-y* plane of 3.03(18) μ_B on the ordered Mn sites only (Mn-3*f*(2) in the representational analysis detailed in ref [13]). The magnetic structure is shown in Figure 7b. The ordered moment at 0.1 K is 60.6% of the maximum 5 μ_B for HS-Mn^{2+} (d^5), compared to 80% (3.2 vs. 4 μ_B) for the same site in $FeFe_3Si_2Sn_7O_{16}$.[13] One small difference is that while the long-range ordered stripes in $FeFe_3Si_2Sn_7O_{16}$ have a pronounced FM component along the Fe-3*f*(2) chains in addition to the AFM component perpendicular to those chains,[13] in $FeMn_3Ge_2Sn_7O_{16}$ the refined FM component was close to zero (0.37(20) μ_B vs. 3.01(17) μ_B for the AFM component): i.e., the zero-field striped structure is non-colinear for $FeFe_3Si_2Sn_7O_{16}$ but nearly colinear for $FeMn_3Ge_2Sn_7O_{16}$. This may reflect the greater anisotropy of octahedral HS-Fe^{2+} (d^6, $t_{2g}^4e_g^2$) vs. HS-Mn^{2+} (d^5, $t_{2g}^3e_g^2$), consistent with the original motivation for this work.

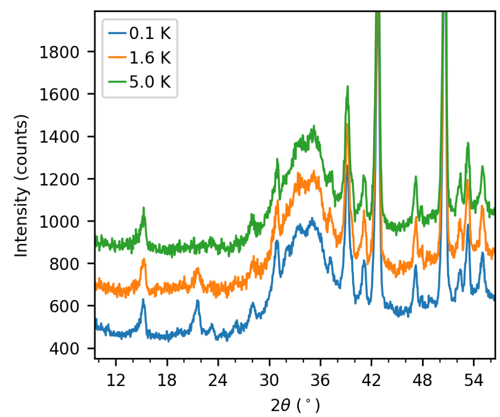

Figure 6. NPD data (λ = 2.4395 Å) for $FeMn_3Ge_2Sn_7O_{16}$ collected at 5 K, 1.6 K, and 0.1 K, focusing on the low-angle region where magnetic scattering is strongest. The broad features (particularly marked at ~35 °2θ) are background from the ^{3}He-dilution insert. The most prominent magnetic Bragg peak to appear below 5 K (marked *) can be indexed to (-1, ½, ½), characteristic of the "striped" magnetic structure of $FeFe_3Si_2Sn_7O_{16}$.[13]

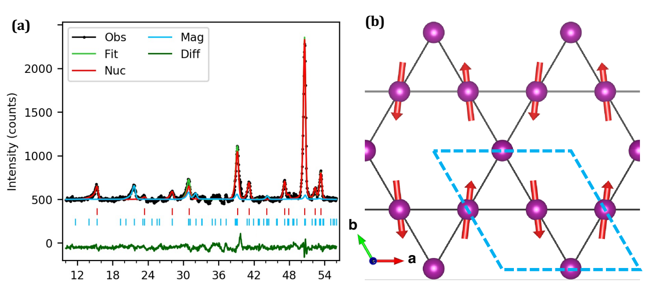

Figure 7. a) Rietveld fit (R_{wp} = 3.13 %) of the nuclear (upper reflection markers) and magnetic (middle reflection markers) structures of $FeMn_3Ge_2Sn_7O_{16}$ to the low-angle region of 2.4395 Å NPD data collected at 0.1 K in zero applied magnetic field. The background and SnO_2 impurity have been subtracted for clarity. **b)** The corresponding magnetic structure, showing only Mn sites in a single kagomé plane (purple spheres) and the refined magnetic moments (red arrows). The nuclear unit cell is shown by dashed blue lines.

To investigate the change in the M-H curve above ~2 T below T_N (Figure 5), field-dependent NPD data were collected at 0.1 K. Data were collected in increasing fields at 0, 1, 4 and 10 T. The field was then returned to 0 T and data were collected at 0, 6, 8 and 10 T. The data are shown in Figure 8. Magnetic Bragg peaks due to the $q = (0,½,½)$ striped state are suppressed above 2 T. As the field is increased further, selected nuclear Bragg peaks grow in intensity, indicating a change to a $q = (0,0,0)$ magnetic state. When the field is released, the change is reversed, but the recovered $q = (0,½,½)$ peaks are greatly broadened; and when the field is increased again, the $q = (0,0,0)$ magnetic intensity is stronger than the first time. Note that the relative intensities of the majority of nuclear Bragg peaks remain constant throughout, ruling out field-induced particle reorientation as an explanation. We tested the possible magnetic structures by Rietveld refinement against the NPD dataset collected at 10 T and 0.1 K, using TOPAS-Academic[17] in combination with ISODISTORT.[18] The best fit was obtained for a model in the space group *C*2'/*m'* (Opechowski-Guccione setting, # 12.5.70), as shown in Figure 9.

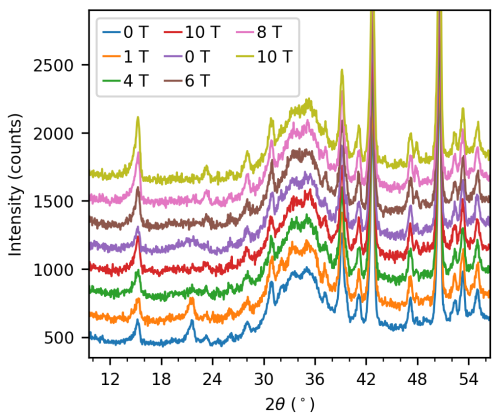

Figure 8. NPD data (λ = 2.4395 Å) for $FeMn_3Ge_2Sn_7O_{16}$ at 0.1 K in successive applied magnetic fields of 0, 1, 4, 10, 0, 6, 8, 10 T, in the low-angle region where magnetic scattering is strongest. The broad features (notably at ~35 °2θ) are background from the ^{3}He-dilution insert. Nuclear Bragg peaks that develop prominent additional magnetic intensity at high applied fields are labelled.

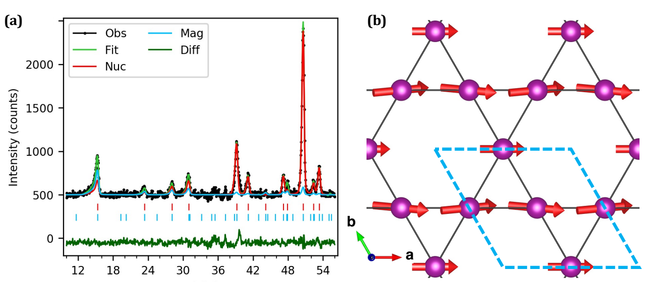

Figure 9. a) Rietveld fit (R_{wp} = 3.67 %) of the nuclear (upper reflection markers) and magnetic (middle reflection markers) structures of $FeMn_3Ge_2Sn_7O_{16}$ to the low-angle region of 2.4395 Å NPD data collected at 0.1 K in a 10 T applied magnetic field. The background and SnO_2 impurity have been subtracted for clarity. **b)** The corresponding magnetic structure, showing only Mn sites in a single kagomé plane (purple spheres) and the refined magnetic moments (red arrows). The nuclear unit cell is shown by dashed blue lines.

Comparing the magnetic structures of $FeMn_3Ge_2Sn_7O_{16}$ at 0.1 K in 0 T and 10 T applied magnetic fields, as shown in Figure 7b and 9b respectively, the relationship and transition between them can be considered. Firstly, and most obviously, the magnetically idle/fluctuating sites in the zero-field "striped" structure show some alignment to give a net ferromagnetic (FM) moment in the high-field structure, which is explained by the external applied field resolving the geometric frustration on that site. Secondly, the long-range ordered stripes have AFM relationships among them along the *x* and *y* axes in the zero-field structure, but FM relationships in the high-field structure (hence the change in *q*-vector); and they also develop FM components parallel to those of the formerly disordered site.

To the best of our knowledge, this Γ_6 $q = (0,0,0)$ magnetic state on a kagomé lattice has not been experimentally observed before, nor theoretically proposed (although the published phase diagrams and models typically do not include Zeeman terms). However, it should be emphasised that the refined magnetic model shown in Figure 9b is not definitive, because the relative intensities of magnetic Bragg peaks in the powder diffraction pattern are calculated on the basis that all domains are randomly oriented. This assumption is undermined for magnetic domains in an oriented external applied field, even if the sample is sufficiently well-packed to prevent reorientation of the grains themselves. Measurements from a large single crystal, which has thus far eluded our synthetic efforts, should ideally be made to confirm and/or improve the model before embarking on a detailed theoretical analysis. Nevertheless, the fact that $FeMn_3Ge_2Sn_7O_{16}$ undergoes a field-induced change in *q* vector, while $FeFe_3Si_2Sn_7O_{16}$ does not, further emphasises that the magnetic interactions in the former are even more finely balanced than the latter.

Conclusions

The hitherto very limited compositional range of the layered structure type $AB_3Si_2Sn_7O_{16}$, where $A = B =$ Fe (i.e., $FeFe_3Si_2Sn_7O_{16}$) was the only stoichiometric example, can be expanded by substituting Ge^{4+} for Si^{4+} in the bridging/stannite layers. Crucially, we have synthesised a second stoichiometric example, $FeMn_3Ge_2Sn_7O_{16}$. This is an important case because the transition metal ions in the kagomé lattice BO_6 octahedral sites have been completely changed from magnetically anisotropic L = 2 HS Fe^{2+} (d^6) to isotropic L = 0 HS Mn^{2+} (d^5). The anisotropic d^6 ($t_{2g}^4e_g^2$) configuration was suspected of playing a role in the 'striped' magnetic structure of $FeFe_3Si_2Sn_7O_{16}$, which breaks trigonal symmetry and leaves 1/3 of the magnetic moments in the kagomé layer geometrically frustrated and magnetically idle/fluctuating down to at least 0.1 K. Our observation of the same striped magnetic structure in $FeMn_3Ge_2Sn_7O_{16}$, in the same temperature range, rules this out as the driving force. However, the fact that the zero-field striped structure is non-colinear for $FeFe_3Si_2Sn_7O_{16}$ but very nearly colinear for $FeMn_3Ge_2Sn_7O_{16}$ may be a consequence of this change in anisotropy on the *B* site.

Considering the crystal-chemical features of the $AB_3(Si,Ge)_2Sn_7O_{16}$ family compared to other kagomé-lattice compounds, the most striking feature is the large separation between the kagomé layers, and the relatively covalent (vs. ionic) character of the intermediate layers. We believe this is the unique feature of the family that helps preserve ideal trigonal symmetry, and hence the geometric frustration on the magnetically disordered *B* site, down to the lowest temperatures we can measure. Finally, we have shown here that an external applied magnetic field can lift the degeneracy on this site and give rise to another ordered magnetic structure never before observed nor predicted on a kagomé lattice. As a unique and potentially much bigger class of compounds than previously thought, the chemistry of the $AB_3(Si,Ge)_2Sn_7O_{16}$ family is clearly deserving of further systematic exploration; and as the most ideal case discovered so far, the low-temperature behaviour of $FeMn_3Ge_2Sn_7O_{16}$ in particular calls for more detailed experimental and theoretical study.

AUTHOR INFORMATION

Corresponding Author

* chris.ling@sydney.edu.au

Author Contributions

The manuscript was written through contributions of all authors. All authors have given approval to the final version of the manuscript.

ACKNOWLEDGMENT

This work was supported by the Australian Research Council – Discovery Projects, the Alexander von Humboldt Foundation (Friedrich Wilhelm Bessel Research Award), Deutsche Forschungsgemeinschaft (project B01 of SFB1143, project-id 247310070), the Japan Society for the Promotion of Science (International Research Fellowship L19533), and the University of Auckland School of Chemical Sciences (FRDF funding, Project #3704173).

ABBREVIATIONS

ADP, atomic displacement parameter; AFM, antiferromagnetic; GFM, geometrically frustrated magnetism; FC, field-cooled; IR, effective ionic radius; NPD, neutron powder diffraction; QSL, quantum spin-liquid; XRPD, X-ray powder diffraction; ZFC, zero field-cooled.

REFERENCES

1. Anderson, P. W., Resonating valence bonds: A new kind of insulator? *Materials Research Bulletin* **1973,** *8* (2), 153-160.
2. Zhou, Y.; Kanoda, K.; Ng, T.-K., Quantum spin liquid states. *Reviews of Modern Physics* **2017,** *89* (2), 025003.
3. Shimizu, Y.; Miyagawa, K.; Kanoda, K.; Maesato, M.; Saito, G., Spin Liquid State in an Organic Mott Insulator with a Triangular Lattice. *Physical Review Letters* **2003,** *91* (10), 107001.
4. Nakatsuji, S., Spin Disorder on a Triangular Lattice. *Science* **2005,** *309* (5741), 1697-1700.
5. Feng Yuan, P.; Shen, L.; Yang, M.; Wang, A.; Zeng, M.; Wu, Q.; Chintalapati, S.; Chang, C. R., Prospects of spintronics based on 2D materials. *Wiley Interdisciplinary Reviews: Computational Molecular Science* **2017,** *7* (5), e1313.
6. Nocera Daniel, G.; Bartlett Bart, M.; Grohol, D.; Papoutsakis, D.; Shores Matthew, P., Spin Frustration in 2D Kagomé Lattices: A Problem for Inorganic Synthetic Chemistry. *Chemistry – A European Journal* **2004,** *10* (16), 3850-3859.
7. Atwood, J. L., A molecular toolkit for magnetism. *Nature Materials* **2002,** *1* (2), 91-92.
8. Balents, L., Spin liquids in frustrated magnets. *Nature* **2010,** *464* (7286), 199-208.
9. Savary, L.; Balents, L., Quantum spin liquids: a review. *Reports on Progress in Physics* **2016,** *80* (1), 016502.
10. Knolle, J.; Moessner, R., A Field Guide to Spin Liquids. *Annual Review of Condensed Matter Physics* **2019,** *10* (1), 451-472.
11. Harris, A. B.; Kallin, C.; Berlinsky, A. J., Possible Néel orderings of the Kagomé antiferromagnet. *Physical Review B* **1992,** *45* (6), 2899-2919.
12. Söhnel, T.; Böttcher, P.; Reichelt, W.; Wagner, F. E., Fe4Si2Sn7O16: A combination of FeSn6-octahedra with layers of (Fe3Sn)O6-octahedra; Preparation, properties, and crystal structure. *Zeitschrift fur Anorganische und Allgemeine Chemie* **1998,** *624* (4), 708-714.
13. Ling, C. D.; Allison, M. C.; Schmid, S.; Avdeev, M.; Gardner, J. S.; Wang, C. W.; Ryan, D. H.; Zbiri, M.; Söhnel, T., Striped magnetic ground state of the kagome lattice in Fe4Si2Sn7O16. *Physical Review B* **2017,** *96* (18), 180410.
14. Dengre, S.; Sarkar, R.; Opherden, L.; Herrmannsdörfer, T.; Allison, M.; Söhnel, T.; Ling, C. D.; Gardner, J. S.; Klauss, H. H., Magnetic anisotropy and spin dynamics in the kagome magnet Fe4Si2Sn7O16: NMR and magnetic susceptibility study on oriented powder. *Physical Review B* **2021,** *103* (6), 064425.
15. Allison, M. C.; Avdeev, M.; Schmid, S.; Liu, S.; Söhnel, T.; Ling, C. D., Synthesis, structure and geometrically frustrated magnetism of the layered oxide-stannide compounds Fe(Fe3−xMnx)Si2Sn7O16. *Dalton Trans.* **2016,** *45*, 9689-9694.
16. Shannon, R., Revised effective ionic radii and systematic studies of interatomic distances in halides and chalcogenides. *Acta Crystallographica Section A* **1976,** *32* (5), 751-767.
17. Coelho, A., TOPAS and TOPAS-Academic: an optimization program integrating computer algebra and crystallographic objects written in C++. *Journal of Applied Crystallography* **2018,** *51* (1), 210-218.
18. Campbell, B. J.; Stokes, H. T.; Tanner, D. E.; Hatch, D. M., ISODISPLACE: a web-based tool for exploring structural distortions. *Journal of Applied Crystallography* **2006,** *39* (4), 607-614.
19. Liss, K.-D.; Hunter, B.; Hagen, M.; Noakes, T.; Kennedy, S., Echidna—the new high-resolution powder diffractometer being built at OPAL. *Physica B: Condensed Matter* **2006,** *385*, 1010-1012.
20. Kamusella, S.; Klauss, H.-H., Moessfit. *Hyperfine Interactions* **2016,** *237* (1), 82.
21. Stevanović, M. M., Evaluation of the temperature dependence of vapour pressure for silicon and germanium. *Thermochimica Acta* **1984,** *77* (1), 167-176.
22. Chen, Y.-L.; Yang, D.-P., Mössbauer effect in lattice dynamics. **2007**, Weinheim: Wiley-VCH. p 79-111.
23. Bain, G. A.; Berry, J. F., Diamagnetic Corrections and Pascal's Constants. *Journal of Chemical Education* **2008,** *85* (4), 532.

TOC Graphic

$FeMn_3Ge_2Sn_7O_{16}$ features a perfectly hexagonal kagomé lattice of isotropic (high-spin d^5, L = 0) Mn^{2+} cations. Below 2.2 K it adopts a “striped” antiferromagnetic structure in which one-third of the spins are geometrically frustrated and continue to fluctuate down to at least 0.1 K in an apparent partial spin-liquid state. This frustration can be overcome by applying a substantial external magnetic field.